Article

A Multi-Scale Flood Monitoring System Based on Fully Automatic MODIS and TerraSAR-X Processing Chains

Sandro Martinis *, André Twele, Christian Strobl, Jens Kersten and Enrico Stein

German Remote Sensing Data Center (DFD), German Aerospace Center (DLR), Oberpfaffenhofen, D-82234 Wessling, Germany; E-Mails: andre.twele@dlr.de (A.T.); christian.strobl@dlr.de (C.S.); jens.kersten@dlr.de (J.K.); enrico.stein@dlr.de (E.S.)

* Author to whom correspondence should be addressed; E-Mail: sandro.martinis@dlr.de; Tel.: +49-8153-28-3034; Fax: +49-8153-28-1445.

Abstract: A two-component fully automated flood monitoring system is described and evaluated. This is a result of combining two individual flood services that are currently under development at DLR's (German Aerospace Center) Center for Satellite based Crisis Information (ZKI) to rapidly support disaster management activities. A first-phase monitoring component of the system systematically detects potential flood events on a continental scale using daily-acquired medium spatial resolution optical data from the Moderate Resolution Imaging Spectroradiometer (MODIS). A threshold set controls the activation of the second-phase crisis component of the system, which derives flood information at higher spatial detail using a Synthetic Aperture Radar (SAR) based satellite mission (TerraSAR-X). The proposed activation procedure finds use in the identification of flood situations in different spatial resolutions and in the time-critical and on demand programming of SAR satellite acquisitions at an early stage of an evolving flood situation. The automated processing chains of the MODIS (MFS) and the TerraSAR-X Flood Service (TFS) include data pre-processing, the computation and adaptation of global auxiliary data, thematic classification, and the subsequent dissemination of flood maps using an interactive web-client. The system is operationally demonstrated and evaluated via the monitoring two recent flood events in Russia 2013 and Albania/Montenegro 2013.

Keywords: TerraSAR-X; MODIS; flood; disaster; automatic thresholding; fuzzy logic; Web GIS; multi-scale monitoring; cloud shadow modeling

1. Introduction

The application of satellite captured earth observation imagery for monitoring and mapping flood events has proven useful in numerous crisis situations. High resolution Synthetic Aperture Radar (SAR) data from the satellite missions TerraSAR-X, Radarsat-2, and the Cosmo-SkyMed constellation (CSK) have been increasingly employed by commercial and non-commercial entities for the derivation of detailed and valuable information on inundation extent in flood affected during rapid mapping activities. The potential of these data has been demonstrated by several previous investigations to support flood emergency situations [1–8].

The aforementioned satellite systems do not possess systematic data acquisition capabilities but need to be programmed to capture data over a defined Area Of Interest (AOI). Due to this steering capability of the satellite, the time span between two consecutive data acquisitions over a defined region on the Earth's surface can be significantly lower than the nominal repetition rate of the satellite system. In unfavorable conditions there is a considerable time span between satellite programming and acquisition time. This depends on the uplink and downlink situation between ground stations and the satellite, the geographic latitude of the AOI and the selected spatial resolution of the data and the swath width of the sensor.

Apart from the described satellite characteristics and considerations that govern communication and control, arguably the most critical consideration for rapid mapping activities is that the satellite programming should be performed at the earliest possible opportunity. In the context of flood events, this may already be when specific observable criteria regarding inundation are reached, with a plausible worsening of the situation.

Data acquisitions are frequently triggered when disaster management authorities request the service of rapid mapping entities or mechanisms, such as the International Charter of Space and Major Disasters [9]. Unfortunately, in many cases, such satellite-based emergency response mechanisms are not activated until a disaster situation has already become severe. This may lead to data acquisitions being too late to capture the peak of the flood. In the worst case, the flood has already completely receded when the first scene is being recorded. In this context, a system that continuously monitors parts of the Earth's surface could assist to optimize the time-critical, on demand programming of high-resolution SAR satellite acquisitions at an early stage of an evolving flood situation.

Over the last decade, the utility of medium-resolution optical data, such as MODIS for inundation mapping and monitoring, has been demonstrated in numerous flood events by the work of the Dartmouth Flood Observatory [10]. Building upon this work, NASA's Goddard's Office of Applied Science proposed an automated global daily flood and surface water mapping service [11], which is still in development. As one of the first SAR-based operational services, the Fast Access to Imagery for Rapid Exploitation (FAIRE) service, hosted on the European Space Agency's (ESA) Grid Processing on Demand (G-POD) system [12], provides automatic SAR pre-processing and change detection capabilities which can be triggered on demand by a user via a web-interface. The FAIRE online application is currently being extended with flood mapping capabilities, based on a comparison of SAR data acquired during crisis situations with corresponding archive/reference data acquired at normal water levels. Recently, Westerhoff *et al.* [13] presented an automated method to derive inundation probabilities from globally acquired Envisat ASAR Wide Swath data. An extension to

systematic data acquisitions, via the forthcoming Sentinel-1 mission, is envisaged for the aforementioned services. Several studies integrate SAR and optical data for flood mapping in SensorWeb environments, e.g., in [14] a SensorWeb to generate real-time flood maps in the Thailand Central Plain is proposed, based on Radarsat and MODIS data. In [15], a Namibia SensorWeb flood early warning pilot project is described which is mainly based on data of the EO-1, MODIS, and Radarsat satellites. To the knowledge of the authors, there exists no system which uses the near real-time classification result of a systematically acquiring satellite mission of high temporal frequency to optimize the time-critical on demand programming of high resolution SAR satellite acquisitions for detailed flood monitoring.

In this contribution, a fully automated multi-scale flood monitoring system is presented. The system combines two individual fully automated flood mapping services that are currently under development at the German Aerospace Center's (DLR) Center for Satellite based Crisis Information (ZKI). The monitoring component of the system systematically derives flood extents on a continental scale using an optical medium resolution satellite sensor at a high temporal resolution. Based on these results, a high-resolution satellite system is triggered based on an automatic E-mail or SMS alert over flood affected areas to derive crisis information in high detail. The monitoring component of this service is based on data of the Moderate Resolution Imaging Spectroradiometer (MODIS) on NASA's Terra satellite, and provides information about evolving flood situations, even in large-scale watersheds on a national to continental scale (spatial resolution 250 m). Based on a flood alert derived from the MODIS processing chain, or other information sources, a fully automated flood service based on DLR's Synthetic Aperture Radar satellite mission TerraSAR-X [16] can be triggered on demand to derive higher detail on the flood situation at local to regional scales.

The fully automated processing chains of the MODIS Flood Service (MFS) and the TerraSAR-X flood service (TFS) including the pre-processing of the satellite data, the computation and adaption of global auxiliary data (digital elevation models, topographic slope information, and reference water masks), unsupervised initialization of the classification, post-classification refinement, and dissemination of the crisis information via a web-based user interface are described. The processing chains were implemented within a service-oriented architecture, based on the Open Geospatial Consortium (OGC) compliant Web Processing Service (WPS). The open source software PyWPS was used as the implementing software. A more technical description of the WPS implementation with PyWPS is out of the scope of this paper and is given in [17].

The operational efficiency of the proposed flood mapping system is described via two recent flood event activations in Russia (2013) and Albania/Montenegro (2013).

2. Methodology

A detailed workflow of the proposed multi-scale flood monitoring system is given in Figure 1. In this chapter the processing chains of the MODIS (Section 2.1) and TerraSAR-X Flood Service (Section 2.2) are presented highlighting the pre-processing of the satellite and auxiliary datasets, the thematic flood analysis, and the dissemination of the classification results via a web-based user interface.

Figure 1. The MODIS and TerraSAR-X processing chains of the proposed multi-scale flood monitoring system.
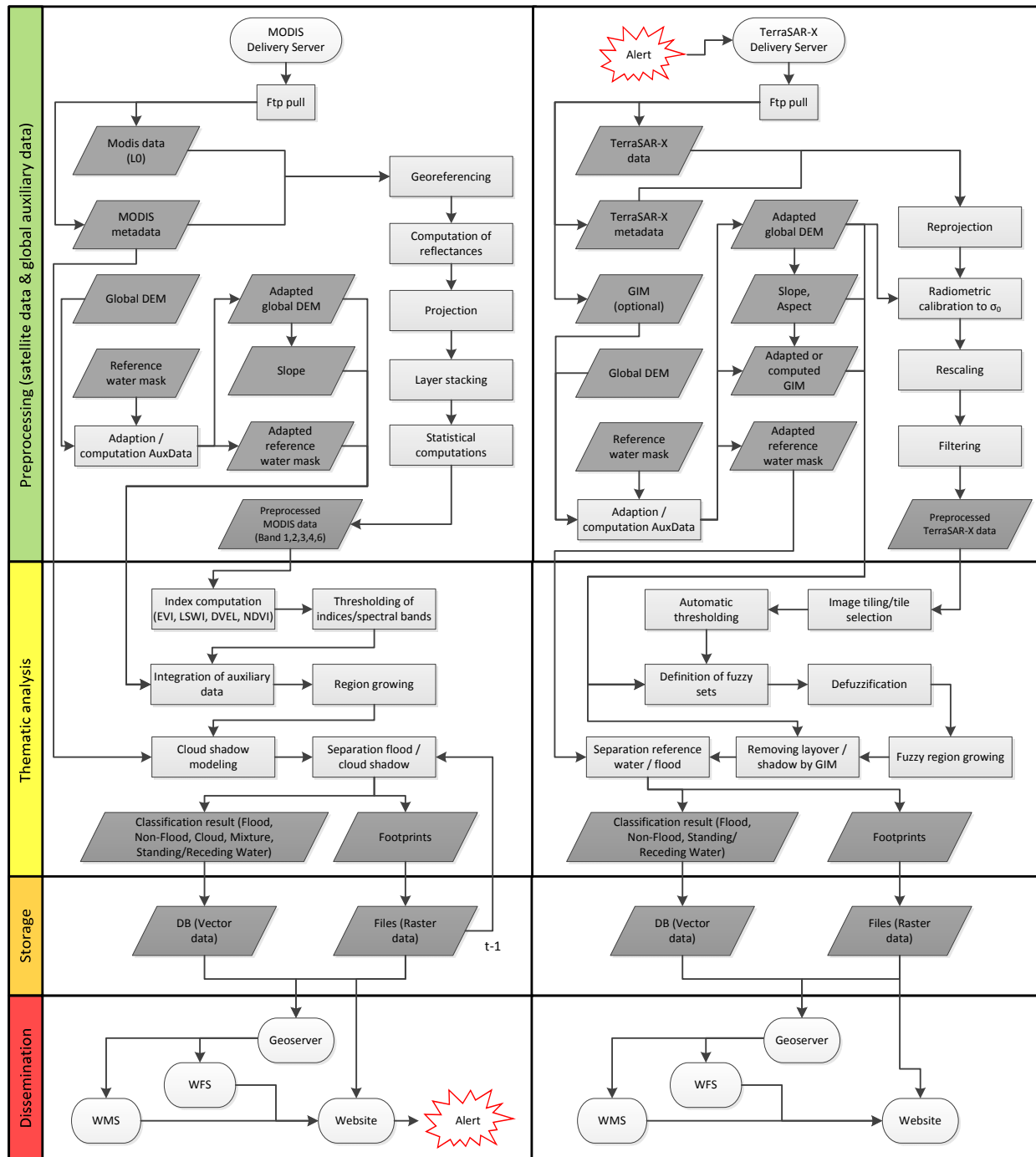
2.1. MODIS Flood Service

2.1.1. Pre-Processing of MODIS and Auxiliary Data

Direct broadcast MODIS data are received by satellite downlink stations at DLR institutions in Oberpfaffenhofen and Neustrelitz, Germany. The spatial extent of the received MODIS data covers the

whole of Europe as well as parts of Western Asia and Northern Africa. Six gigabytes of MODIS data are received daily, which are converted from raw form (Level 0) to Level 1B data according to the NASA pre-processing specifications MOD 01, and archived in the DLR's Data Information and Management System (DIMS). The monitoring component of the flood mapping system directly acquires the Level 0 datasets received and independently pre-processes selected bands of the data to maintain computational efficiency. Flood masks are calculated based on MODIS bands one through four and band six (Table 1). Bands 1 (ρ_{RED}) and 2 (ρ_{NIR}) have a ground resolution of 250 m while bands 3 (ρ_{BLUE}), 4 (ρ_{GREEN}), and 6 (ρ_{SWIR}) have a ground resolution of 500 m.

Table 1. Moderate Resolution Imaging Spectroradiometer (MODIS) bands [18] (1–4, 6) used in the flood detection system.

| Band	Bandwidth (nm)	Resolution (m)	Primary Use
1 (ρ_{RED})	620–670	250	Absolute Land Cover Transformation, Chlorophyll
2 (ρ_{NIR})	841–876	250	Cloud Amount, Vegetation Land Cover Transformation
3 (ρ_{BLUE})	459–479	500	Soil/Vegetation Differences
4 (ρ_{GREEN})	545–565	500	Green Vegetation
6 (ρ_{SWIR})	1628–1652	500	Snow/Cloud Differences

Level 1A (MOD 01), Level 1B (MOD 02), and Geolocation Datasets (MOD 03)

During the first pre-processing steps the Level 1A Radiance Counts (MOD 01), the Geolocation dataset (MOD 03), and finally the Level 1B Calibrated Geolocated Radiances (MOD 02) are calculated. The Level 1A Radiance contains counts for the 36 MODIS channels, along with raw instrument engineering and spacecraft ancillary data. The data are used as input for geolocation, calibration, and processing. The Level 1B calibrated Geolocation dataset consists of the calibrated and geolocated at-aperture radiances (W/(m^2 μm sr)) for 36 bands generated from MODIS Level 1A sensor counts (Figure 2a). The Geolocation dataset contains geodetic coordinates, ground elevation, solar and satellite zenith and azimuth angles for each MODIS 1 km sample. These data are provided as a companion dataset to the Level 1B calibrated radiances and the Level 2 datasets to enable further processing [18]. The processing for these three products occurs within the SeaWiFS Data Analysis System [19] and includes the product levels MOD 01–03.

MODIS Level 2 Corrected Reflectance Product

During this pre-processing step MODIS Level 2 corrected reflectances are calculated from the MODIS Level 1B calibrated radiances (see Figure 2b). The processing is performed by the MODIS Corrected Reflectance Science Processing Algorithm (CREFL_SPA), provided by the NASA Direct Readout Laboratory (DRL). CREFL_SPA creates a MODIS Level 2 Corrected Reflectance product. A simple atmospheric correction of MODIS visible, near infrared, and short-wave infrared bands (Bands 1–16) is used. It requires no real-time input of ancillary data. The Corrected Reflectance products are comparable to the MODIS Land Surface Reflectance product (MOD 09) in clear atmospheric conditions [20].

Figure 2. Example of (**a**) the corrected radiances in the range of 0 to 65,535 and (**b**) the projected corrected reflectances in the range from 0 to 10,000 from MODIS Bands 1–3 and 6. Extent: (UL) 63°01'10.0"N, 31°26'15.0"E; (LR) 30°26'48.0"N, 50°58'50.0"E.

(**a**)

(**b**)
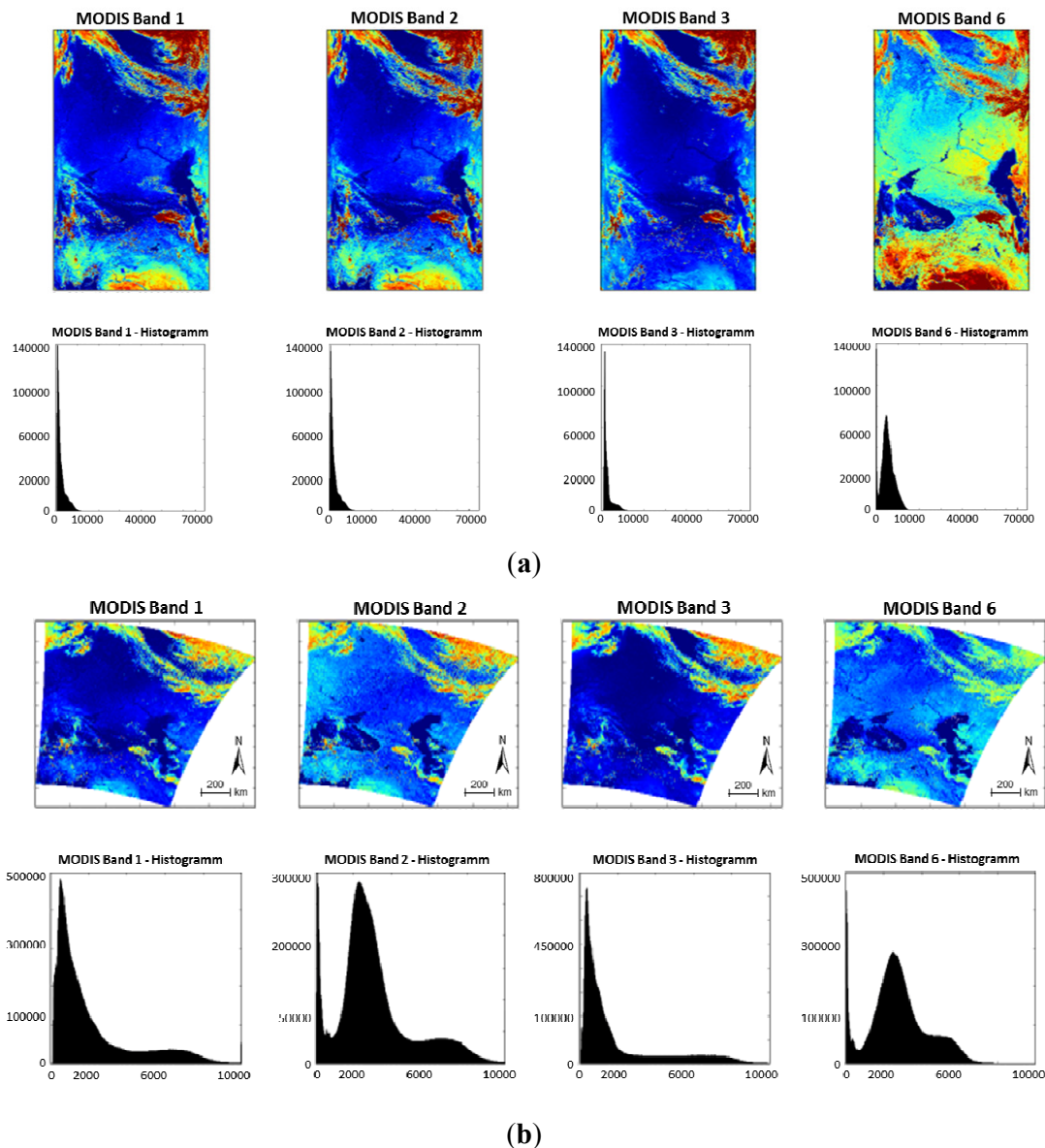
Projection

The swath dimensions of MODIS data are 2,330 km (across track) by 10 km (along track at nadir), giving it the capability to cover the entire globe every one to two days. In contrast to other scanning sensors, MODIS observes, within one scan, ten lines of 1 km spatial resolution (40 lines of 250 m resolution and 20 lines of 500 m resolution, respectively). The projection of the swath to grid data is accomplished by using the MODIS Swath Reprojection Tool (MRTSwath). MRTSwath provides the capability to transform MODIS Level 1B and Level 2 data from swath format to a uniformly gridded image that is geographically referenced according to user-specified projection and resampling parameters [21].

Post-Processing with GDAL

The three result datasets (reflectances of the 250 m and 500 m resolution bands and the geolocation file) are post-processed with the GDAL software. This process encompasses the stacking of the layers, assigning "nodata" values, and the calculation of the layer statistics.

Auxiliary Datasets

In order to enable the distinction between persistent water bodies and flooded areas, the Global Raster Water Mask (MOD44W) [22], with a 250 m spatial resolution, is used. As the MOD44W product was generated using MODIS data from 2000 to 2007, it is temporally static and therefore does not provide an indication of normal seasonal water fluctuations [23]. As the proposed pre-operational service focuses mainly on Europe, seasonal influences are comparably low. The ASTER Global Digital Elevation Model Version 2 (GDEM V2) [24], with a spatial resolution of one arc second, is employed to refine the flood mask. Slope information $s_{(x,y)}$ in degrees for each pixel (x,y) are computed (local steepness of terrain) according to

$$s_{(x,y)} = arctan\left(\sqrt{\left(\frac{\Delta x_{(x,y)}}{n \cdot r_x}\right)^2} + \sqrt{\left(\frac{\Delta y_{(x,y)}}{n \cdot r_y}\right)^2}\right) \cdot \frac{180}{\pi} \tag{1}$$

where Δx and Δy are the result of a standard Sobel edge filter [25] applied on the DEM taking into account $n = 8$ pixel values (resulting from a 3×3 kernel). r_x, r_y denotes the pixel resolution of the DEM in the x and y directions. The auxiliary datasets are resampled and clipped with respect to the pixel size, extent and location of each MODIS scene.

2.1.2. Thematic Analysis

The thematic analysis comprises the classification of the MODIS data into six output classes, namely "Flood", "Non-flood", "Receding Water", "Standing Water", "Mixture", and "Clouds" (Figure 3). The classification process is separated into the following processing steps:

- Computing of spectral indices
- Initial thresholding of the spectral bands and indices
- Post-processing including the integration of auxiliary data
- Region growing
- Improved separation between water and cloud shadows

Computing of Spectral Indices

The spectral indices EVI (Enhanced Vegetation Index), LSWI (Land Surface Water Index) and DVEL (Difference value between EVI and LSWI) are computed from MODIS spectral Bands 1–3 and 6. These indices have been successfully applied for water detection based on MODIS data in several studies [26–28]:

$$EVI = G \times \frac{\rho_{NIR} - \rho_{RED}}{\rho_{NIR} + C_1 \times \rho_{RED} - C_2 \times \rho_{BLUE} + L} \tag{2}$$

$$LSWI = \frac{\rho_{NIR} - \rho_{SWIR}}{\rho_{NIR} + \rho_{SWIR}} \tag{3}$$

$$DVEL = EVI - LSWI \tag{4}$$

G is a given gain factor, L is a canopy background adjustment factor, C_1 and C_2 are coefficients of the aerosol resistance term, which uses ρ_{BLUE} to correct for aerosol influences in ρ_{RED}. The values of the parameters in the computation of the EVI are defined as $G = 2.5$, $L = 1$, $C_1 = 6$, $C_2 = 7.5$ according to [29,30].

Initial Thresholding of the Spectral Bands and Indices

A preliminary threshold based classification is performed built on an approach originally developed by Sakamoto *et al.* [26] and revised by Islam *et al.* [27], who propose a decision tree procedure to assign each image element to the temporary class "Water-related" and the output classes "Non-flood", "Flood", and "Mixture". The thresholding can be summarized as follows (Figure 3):

- Determination of cloud-cover areas based on a threshold of ≥0.27 from the blue reflectance band. The cloud positions are subsequently used for a geometry-based detection of cloud shadows.
- Classification of non-flooded areas by using an EVI >0.3.
- Initial identification of water-related pixels based on the derived indices using two criteria, which combine the EVI (≤0.3) and the DVEL (≤0.05), as well as the EVI (≤0.05) and the LSWI (≤0.0) respectively.
- Separation of water-related areas into flood surfaces (EVI ≤ 0.1) and mixed pixels (0.1 < EVI ≤ 0.3). A mixed pixel denotes a pixel that contains more than one thematic land-cover element of interest, which is a common phenomenon in moderate resolution MODIS data.

The following post-processing steps are integrated into the classification process to improve the accuracy of the initial classification result derived by the approach described in [26,27].

Post-Processing Including the Integration of Auxiliary Data

Information derived from the ASTER GDEM V2 is employed to reduce the number of misclassified water-related pixels in areas where the plausibility for a flood occurrence is low due to topographic considerations. Areas of steep incline (>10°), or significant height (>2,000 m and a slope of >8.0°), are removed from the flood mask.

Region Growing

Two region growing steps are applied for a refinement of the classification accuracy by relaxing the thresholds in the neighborhood of the initial flood classification result. In the first region growing step image elements of the classes "Flood" or "Mixture" are used as seeds. Neighboring image elements of the class "Non-flood" are assigned to the class "Water-related" by using the following criteria: EVI ≤ 0.31 and DVEL ≤ 0.07 or EVI ≤ 0.06 and LSWI ≤ 0.1. The grown area is subsequently separated into the classes "Mixed" (0.1 < EVI ≤ 0.3) and "Flood" (EVI ≤ 0.1). The second region growing step is used to increase the spatial homogeneity of flooded areas by dilating preliminary

extracted flood surfaces and assigning pixels of the class "Mixture" with a LSWI ≤ 0.08 to the class "Flood". Flood pixels with neighboring mixed pixels are used as seeds.

Figure 3. Flowchart of the thematic MODIS flood processor.
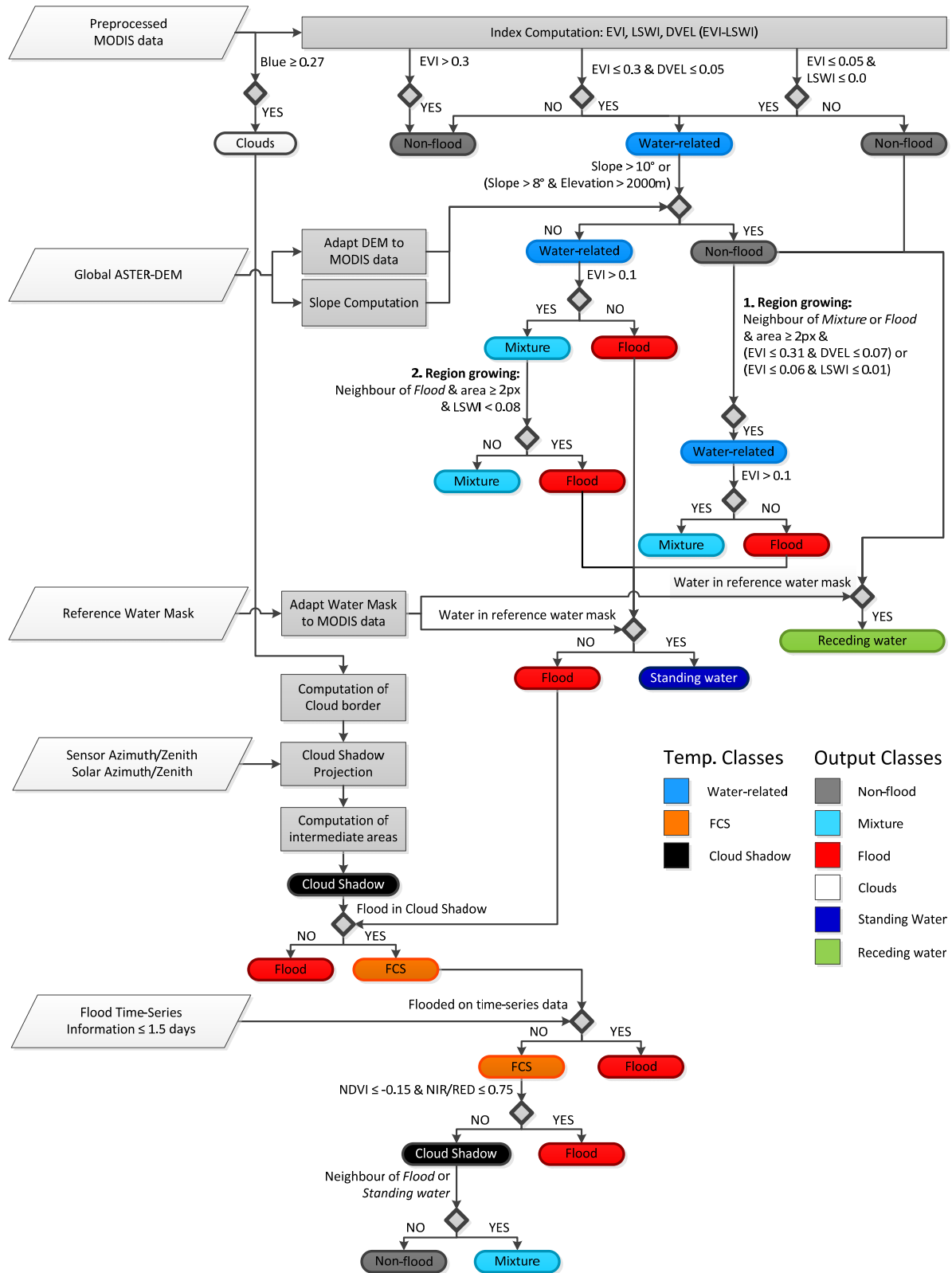
Improved Separation between Water and Cloud Shadows

Cloud shadows are a major problem when monitoring water surfaces using optical remote sensing data, especially in coarse/moderate resolution satellite data. As cloud shadows and water have similar spectral properties, the classification by means of spectral information alone could lead to a significant overestimation of water surfaces near clouded areas. An overview of methods that improve the classification in optical satellite data by detecting cloud shadows can be found in [31,32]. We implemented an approach for separating water and cloud shadows by combining geometrical, spectral, as well as temporal information.

In a first step, a geometry-based technique described in [33] is employed to estimate the position of cloud shadows based on 2D-location (x_{img}, y_{img}) and height (top and bottom) above the surface h_c of the cloud, the solar and viewing zenith angles, θ_s and θ_v, respectively, and the solar and viewing azimuth angles, Φ_s and Φ_v, respectively. Assuming a cloud pixel position (x_{img}, y_{img}), the projection of the cloud on the earth surface is defined by (x_{nadir}, y_{nadir}):

$$x_{nadir} = x_{img} + h_c tan\theta_v sin(\Phi_v + \gamma) \tag{5}$$

$$y_{nadir} = y_{img} + h_c tan\theta_v cos(\Phi_v + \gamma) \tag{6}$$

The projection of the cloud shadow on the ground is then determined by (x_{shadow}, y_{shadow}):

$$x_{shadow} = x_{nadir} - h_c tan\theta_s sin(\Phi_s + \gamma) \tag{7}$$

$$y_{shadow} = y_{nadir} - h_c tan\theta_s cos(\Phi_s + \gamma) \tag{8}$$

where γ is the azimuth angle of the true North from the y axis. The solar and sensor zenith and azimuth angles are captured along with the MODIS data at a 1 km spatial resolution. Equations (7) and (8) approximate a flat surface. A more complex formulation considering the Earth curvature can be found in [32]. For a detailed identification of the cloud shadow positions the availability of information on the cloud top and bottom height is necessary [34]. To be independent from the availability of external data sources during rapid flood mapping activities, simplified assumptions for cloud heights are made [31,33,35].

The elevation of clouds may vary considerably depending on the cloud type and also the geographic latitude. The maximal cloud top height decreases with increasing latitude from a mean height of the tropopause from 16 km in tropical regions to 8 km in polar regions [35]. Similar to [31], the upper limit of cloud top height is divided into three classes according to the geographical latitude. For lower latitudes between 30°N–30°S the maximum cloud altitude is set to 16 km, for the mid-latitude between 30°N/S–60°N/S and in the high-latitude between 60°N/S and 90°N/S to 12 km and 8 km, respectively. The cloud bottom height is assumed to be 0 km. Therefore, only the inner and outer border (with a two pixel margin) of the cloud is projected on the ground as shadow. This significantly reduces the computational effort of the algorithm as the extent of the cloud shadow can be estimated by linearly interpolating between the border of the cloud and the border of the projected cloud-shadow.

Due to these simplifying assumptions, the simulated cloud shadow is usually larger in extent than the real cloud shadow. After the cloud shadow computation all pixels classified as flood outside the cloud shadow mask are assigned to the flood class with a high probability. Pixels covered by the

cloud shadow mask are characterized by a lower probability to belong the class "Flood". These image elements are assigned to the temporary class "Flood in Cloud Shadow" (FCS) (Figure 3). Further criteria, based on temporal and spectral information, are used to identify flooded regions within the simulated cloud shadows. If a pixel of the class "FCS" is labeled as flooded in the preceding MODIS classification result, at T-1 with a time distance of <36 h to the acquisition time of the most current MODIS scene at $T0$, it is assumed to belong to the class "Flood". If the pixel is labeled as "Cloud" at T-1, further classification results of T-x of the last 36 h are iteratively integrated into the test. Only these pixels of the class "FCS" are assigned to flood elements, which fulfill the following spectral criterion [31]: NDVI (ratio between the difference and sum of spectral bands ρ_{NIR} and $\rho_{RED} \leq -0.15$ and a ratio of $\rho_{NIR}/\rho_{RED} \leq 0.75$).

In a final step, the separation between flooded regions and standing water areas is performed using the Global Raster Water Mask (MOD44W) at 250 m spatial resolution [22].

2.1.3. Dissemination of Classification Results

The whole processing chain from the MODIS Level 0 file to the flood mask is implemented with an OGC compliant WPS framework (PyWPS). The processing results are stored within a PostGIS raster database for further analysis. Every output class ("Flood", "Non-flood", "Receding Water", "Standing Water", "Mixture", and "Clouds") is automatically deployed as a single web mapping service (WMS) layer set, which is available for 14 days, within the DLR/ZKI MODIS flood application (Figure 4).

Figure 4. Example of the web application with MODIS Terra scenes over Europe on 27 August 2013. Extent: (UL) 66°10'05.0"N, 14°48'31.0"W; (LR) 37°35'29.0"S, 112°04'58.0"E. The enlarged section shows the alert service with a defined area and the available alert settings (immediate per subscription, immediate per overpass, or daily) and types of notifications (E-mail and/or SMS). Extent: (UL) 42°35'01.0"N, 18°33'05.0"E; (LR) 41°10'55.0"N, 21°08'36.0"E.
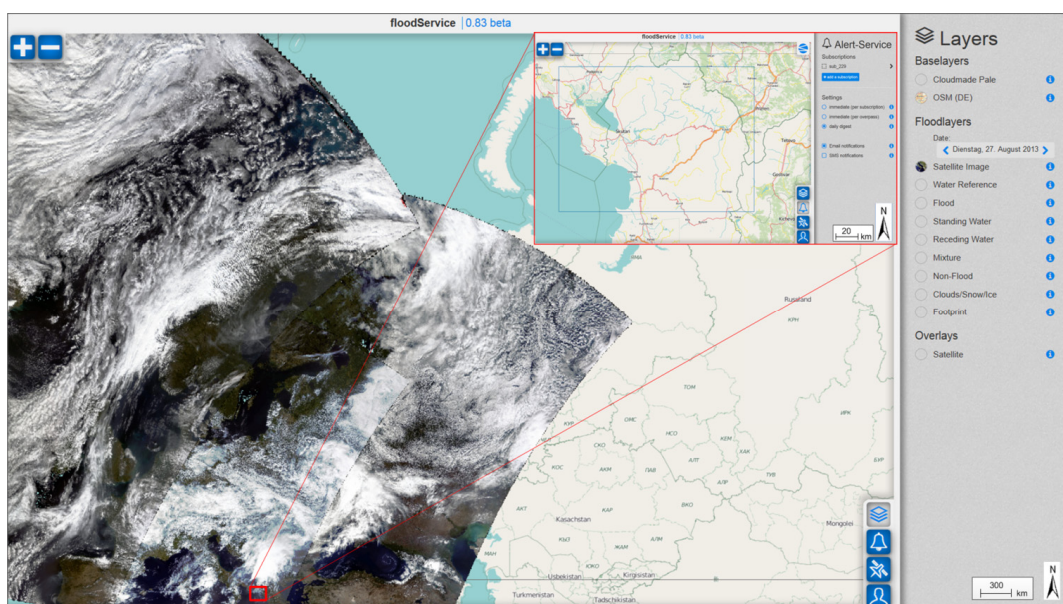
This client is designed for monitoring and viewing the daily results of the MODIS flood processing. A further, and even more important, use case is to receive alerts for user-defined regions or areas of interest. For this purpose a new mobile client is under development, which allows users to select the frequency and method (E-mail, SMS) of information delivery.

The DLR/ZKI is using the described MODIS monitoring service to automatically trigger the TerraSAR-X Flood Service, which derives more detailed information on flood situations at a much finer scale.

2.2. TerraSAR-X Flood Service

Recently several automatic image processing algorithms to derive flooding from SAR data have been proposed [2,5,6,8,36]. Even if the crisis information can be extracted automatically, a certain amount of user interaction is needed for data pre-processing, the collection and adaptation of auxiliary data useful for classification refinement as well as the preparation and dissemination of the crisis information to end users. Martinis *et al.* [16] proposed a fully automated processing chain for near real-time flood detection using high-resolution TerraSAR-X data. The processing chain includes SAR data acquisition, data pre-processing, computing and adapting global auxiliary data, unsupervised initialization of the classification, as well as post-classification refinement by using a fuzzy logic-based algorithm and finally the dissemination of the derived crisis information via a web-based user interface. An outline of these processing steps is given below.

2.2.1. Pre-Processing of TerraSAR-X and Auxiliary Data

The processing chain, starting with downloading and unzipping the enhanced ellipsoid corrected (EEC) amplitude imagery of different acquisition modes (SpotLight, StripMap, ScanSAR) is triggered automatically when a new TerraSAR-X scene is detected on the delivery ftp-server. The imagery and the optional Geocoded Incidence Angle Mask (GIM) are re-projected to WGS84 geographical coordinates (lat/lon) in order to ensure equivalent coordinate systems for all used data products. The GIM is an ancillary dataset, which can be optionally ordered with the EEC product. It provides information about the local incidence angle $\theta_{(x,y)}$ for pixel of the geocoded SAR scene and about the presence of shadow and layover areas [37]. The SRTM water body mask (SWBD) [38] for all regions between 54°S and 60°N, with a resolution of 30 m, as well as the Global Raster Water Mask (MOD44W) at 250 m spatial resolution for all areas which are not covered by SWBD, are used as a reference water mask for the distinction between permanent water bodies and flooded areas. These datasets are extracted and resampled using nearest neighbor resampling for each SAR scene. The ASTER GDEM V2 is incorporated for the refinement of the flood mask and is also used for the optional computation of a GIM [16].

A rigorous radiometric calibration of the digital numbers *DN* of the SAR amplitude data to normalized radar cross section σ_0 (dB) using the GIM is done according to [37]:

$$\sigma_{db}^0 = 10 \cdot log_{10}(k_s \cdot |DN|^2) + 10 \cdot log_{10}\big(sin\theta_{(x,y)}\big) \tag{9}$$

where k_s is a calibration factor. σ_0 is rescaled to a range of (0,400) in order to yield positive values. Finally, a median filter of kernel size 3×3 is applied on the rescaled pixel values for the purpose of speckle reduction and pulse or spike noise removal.

2.2.2. Thematic Analysis

Automatic Tile-Based Thresholding

The fully automated TerraSAR-X flood processor is designed to derive individual scene dependent threshold values for global data acquired with different sensor configurations (*i.e.*, polarization, beam mode, and incidence angle). For this purpose, a parametric tile-based thresholding, proposed in [2], is modified for more robustness and adapted for SAR data, radiometrically calibrated to σ_0 (dB) [16]. The method identifies n image tiles, which are likely to represent a bimodal distribution of the classes to be separated (*i.e.*, water and land surface). The Kittler and Illingworth thresholding approach [39] is used to derive local threshold values τ_n using a cost function, which is based on modeling the sub-histograms of each tile as bi-modal Gaussian mixture distributions. A global threshold, τ_g, is obtained computing the arithmetic mean of the local thresholds. If the derived global threshold exceeds a certain value (e.g., -10 dB) it is assumed that either no water areas exist in the covered region; or the water extent is very small; or water bodies do not appear as dark backscatter regions. This could be due to wind-induced roughening of the water surface or protruding vegetation leading to volume or double bounce scattering of the radar signal. In this case, the threshold τ_g is approximated using an empirically derived linear function depending on the center incidence angle of the SAR scene [16].

Post-Classification

The initial labeling derived by applying the threshold τ_g to the image is further enhanced using a fuzzy logic-based post-classification algorithm. The fuzzy set incorporates SAR backscatter, digital elevation, and slope information, as well as the size of water bodies. The shape of the four membership functions (standard Z and S membership functions) is either determined according to statistical computations or is defined based on empirical studies. The fuzzy thresholds for each function are individually computed for each image element. The corresponding fuzzy elements are combined into one composite fuzzy set by computing the average of the membership degrees of each pixel. The membership degree of the composite fuzzy set is assigned by a membership degree of zero in the event that a single fuzzy element has a membership degree of zero. The flood mask is created in a threshold defuzzification step, which assigns each image element with a membership degree > 0.5 to the class "Flood".

A subsequent region growing step is performed in order to integrate the transient shallow water zone between open flood water surfaces and non-flooded areas. The water bodies extracted by using the defuzzified classification result are used as seeds for dilating the water regions. The water areas are progressively enlarged until a fuzzy logic based tolerance criterion is reached, where only image elements located in the neighbourhood of the flood areas are iteratively scanned.

Finally, the GIM is integrated into the classification process to remove areas incorrectly classified as "flood" due to radar layover and shadowing effects. To differentiate between flooded, standing, and receding water bodies, the classification result is compared to a global reference water mask.

2.2.3. Dissemination of Classification Results

The TerraSAR-X processing chain, starting with the download of the TerraSAR-X amplitude imagery and ending with the derivation of the flood mask, is similar to the MODIS processing chain implemented in the WPS framework. The processing results are stored within a PostGIS Raster database for further analysis. The output classes ("Flood", "Non-flood", "Receding Water", and "Standing Water") are archived as single WMS layers which are interactively accessible via a Web application. The web application is similar to the one illustrated in Figure 4.

3. Experimental Results

3.1. Study Area and Dataset

In this section the multi-scale flood monitoring system based on MODIS and TerraSAR-X data is demonstrated for two recent (2013) flood scenarios in Russia and Albania/Montenegro. For both test cases the acquisition times of MODIS and TerraSAR-X data as well as the triggering times of the TerraSAR-X flood processing chain based on the classification result of the MODIS Flood Service are visualized in Figure 5.

Figure 5. Overview about the times of satellite data acquisitions, flood alerts, and TerraSAR-X ordering for the study areas in Russia and Albania/Montenegro.
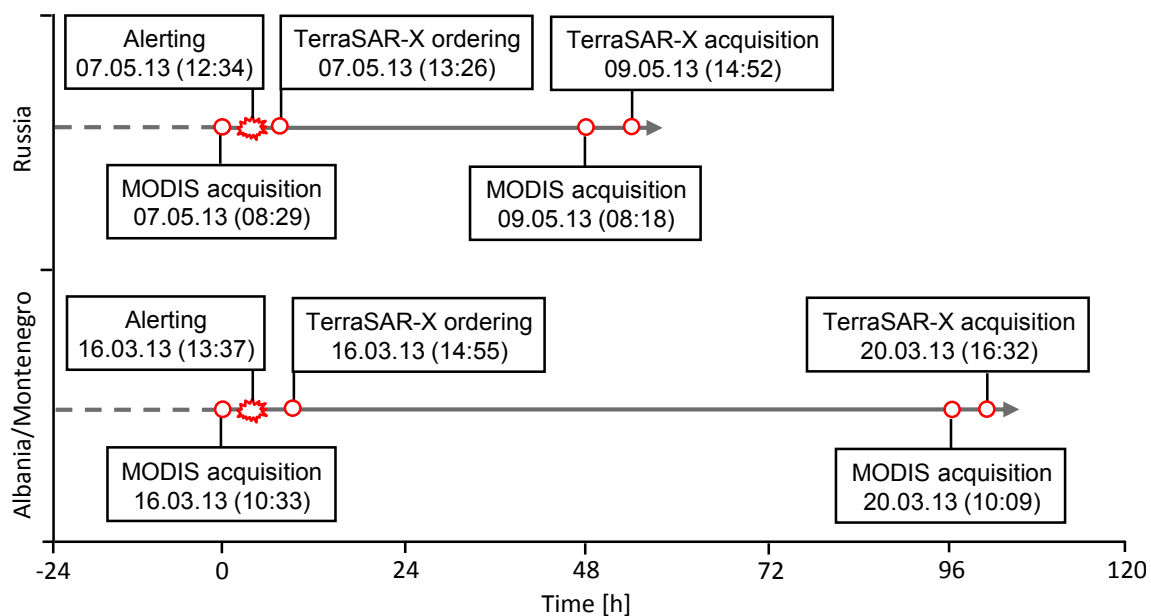
The first test area is situated within Oblast Rjasan, Russia, ~200 km South-East of Moscow. On 7 May 2013 (08:29 UTC) a large-scale flood event around the River Oka was automatically detected in MODIS Terra data by the MODIS flood mapping service. Based on the generated classification results, the TerraSAR-X flood mapping service was triggered. On demand programming resulted in the acquisition of a TerraSAR-X ScanSAR HH polarized scene, five hours after the acquisition of the MODIS scene. The next possible TerraSAR-X acquisition was on 9 May 2013 (14:52 UTC),

approximately two days after triggering the TerraSAR-X Flood Service. A high-resolution flood mask with a spatial resolution of 8.25 m was derived using the automatic processing chain.

The second study area is located in Albania and Montenegro near Lake Scutari. Inundated regions were identified by the MODIS flood processor in the district of Shkoder/Albania and in the northern part of Lake Scutari/Montenegro on 16 March 2013 (08:54 UTC). Based on the flood alert the TerraSAR-X processor was triggered and a ScanSAR HH polarized scene with 8.25 m spatial resolution was ordered (acquisition time: 20 March 2013; 16:32 UTC).

In both scenarios, the MODIS flood mapping service was successful in identifying an evolving flood situation on a large-scale with a medium resolution of 250 m. The MODIS classification output was successfully used for on demand triggering the fully automated TerraSAR-X flood mapping service, which derived high-resolution information on inundation extent of the target areas.

For both test scenarios, high-resolution SAR data would not have been acquired without the identification of the flooding using the MODIS Flood Service.

3.2. Results and Discussion

In this section the classification results of the MODIS and TerraSAR-X Flood Service are quantitatively compared based on two study areas, depicted in Figures 6 and 7. The evaluation is based on the comparison of SAR scenes with the respective closest available MODIS classification results, which are derived from acquisitions on 9 May 2013 (08:18 UTC) for the test area in Russia (~6.5 h before the SAR acquisition) and on 20 March 2013 (10:09 UTC) for the test area in Albania/Montenegro (~6.5 h before the SAR acquisition). Due to the relatively small time-offset of only 6.5 h between SAR and optical data acquisitions, stable flood conditions are assumed for both test scenarios.

The MODIS scenes are resampled and clipped to the pixel spacing and extent of the respective TerraSAR-X scenes. Image elements of the class "Flood" covered by clouds in the MODIS data are removed from the TerraSAR-X flood masks. Each pixel of the SAR imagery is checked against the classification result of the MODIS data and labeled into three classes according to the following criteria: flood detected by TerraSAR-X and MODIS, flood detected only in TerraSAR-X data and flood detected only in MODIS data (Figures 6 and 7). According to quantitative analysis of the TerraSAR-X flood processor in different test sites the overall accuracy of the final flood mask is specified between ~87.5% and ~91.6% in [16]. These values can be used as reference for cross-comparison of the MODIS and TerraSAR-X classification results.

Approximately 47% of the pixels detected as "Flood" in the Russian test area using the SAR data are labeled similarly with the MODIS data. In contrast ~19% are detected as inundated based on the SAR data and ~34% based on the MODIS data. Visually, the flooding within the AOI in Russia is well detected from both sensors and mainly occurs in the neighborhood of River Oka. As can be seen in Figure 6, data from the TerraSAR-X mission can be used to detect even fine details of open flood areas at a local to regional scale due to the high spatial resolution of this radar sensor. In contrast, the relatively coarse resolution of MODIS results in an overestimation of the flood extent within the core of the flood plain. Small water surfaces or flood areas located at the land/water boundary are only

partly detected. These image elements are mainly classified as "mixed pixels" due to mixed reflectance values of the class "Water-related" and non-water or flooded vegetation areas.

Figure 6. Comparison of MODIS Terra and TerraSAR-X classification results (Russia floods, 2013. Extent: (UL) 55°09'04.8"N, 39°12'55.9"E; (LR) 54°11'33.6"N, 41°18'23.5"E).
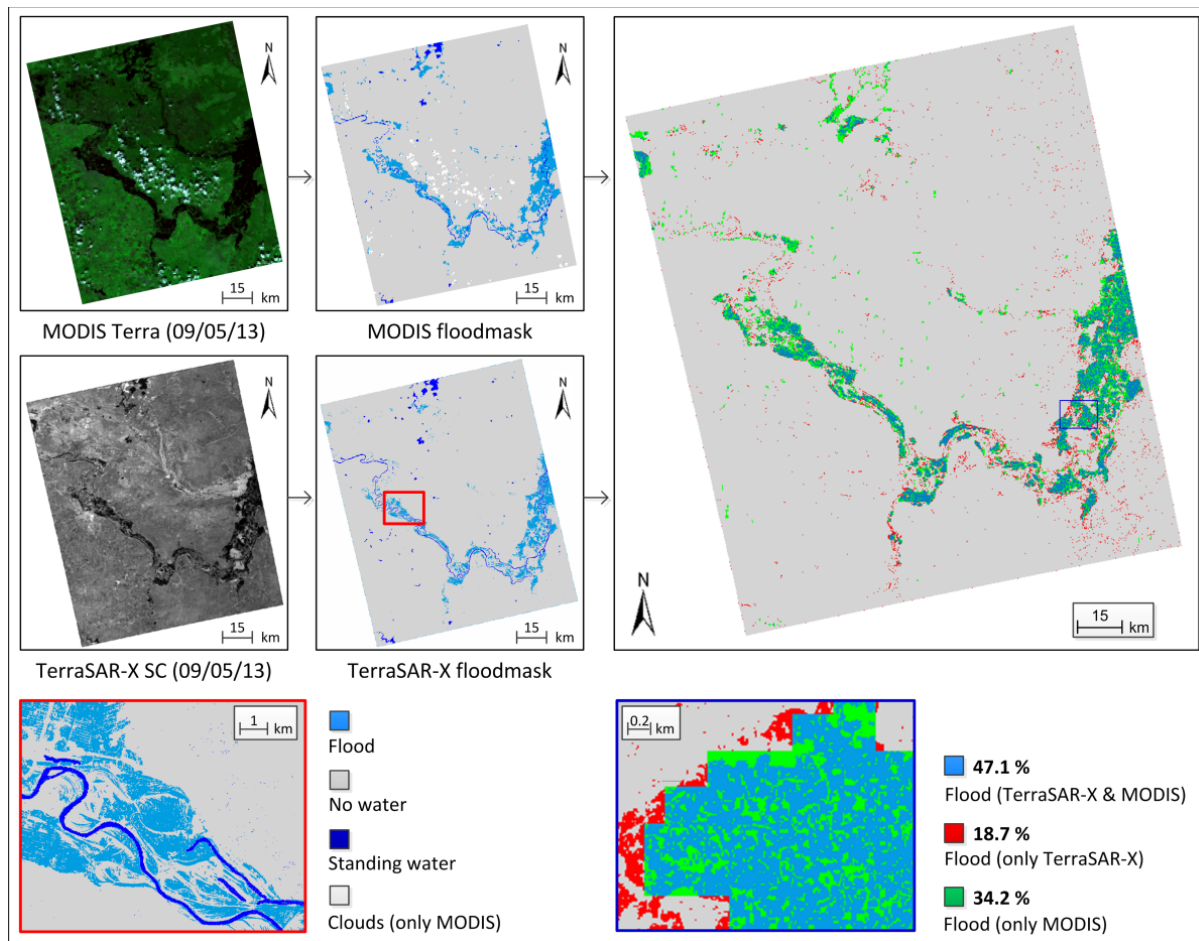

Figure 8a illustrates a scatter plot generated by comparing the MODIS and TerraSAR-X floodmasks on a 2 km grid. The high coefficient of determination ($R^2 = 0.91$) indicates a close agreement between both classification results. The positive deviation of the regression line from the ideal trend line, where $y = x$ is an indicator that more pixels are detected as flooded in MODIS than in the TerraSAR-X data (Figure 8a).

Within the test area in Albania/Montenegro the agreement between MODIS and TerraSAR-X is much lower with a value of only 26.7%. The number of image elements assigned to the class "Flood" based on the data of only one single sensor is much higher. Approximately 36% of the flood extent is detected by TerraSAR-X while 37.6% is detected using the MODIS data. In addition, the correlation of the flood masks between the MODIS and TerraSAR-X derived results on a 2 km grid is much lower with a value of $R^2 = 0.56$ (Figure 8b).

The large differences in classification results between the two areas are explained as follows:

- The flood extent is much smaller for the AOI in Albania/Montenegro. Therefore, MODIS data could only be used for a rough estimation of the actual flood extent. The MODIS derived flood mask is considerably underestimated since mixed areas are very prevalent. In contrast it is possible to derive detailed information about the flooding and to map even small tributaries with an extent lower the spatial resolution of the MODIS images using TerraSAR-X. Therefore, the number of flood pixels identified by TerraSAR-X data only is nearly 17% higher compared to the test site in Russia.

- In comparison to the test area in Russia the cloud coverage at the time of the MODIS acquisition is much higher. Cloud shadows are partly located over flood-affected areas. This leads to an underestimation of the MODIS-derived flood extent due to the reduced spectral separability of water surfaces and cloud shadow areas.

- In the northern part of Lake Scutari in Montenegro, the flooding is extensively covered with vegetation. The X-band SAR signal is very sensitive to flooded vegetation in this region due to the double bounce effect between the water surface and the lower parts of the vegetation. This results in a very high signal return and consequently an underestimation of the flood extent. In contrast the MODIS flood processor is less sensitive to protruding vegetation and is able detect more flood surfaces in this region. This explains the high percentage of flood pixels derived by using the MODIS data (see Figure 7).

Figure 7. Comparison of MODIS Terra and TerraSAR-X classification results (Albania/Montenegro floods, 2013. Extent: (UL) 42°29'01.3"N, 18°34'57.5"E; (LR) 41°48'29.7"N, 20°05'54.1"E).
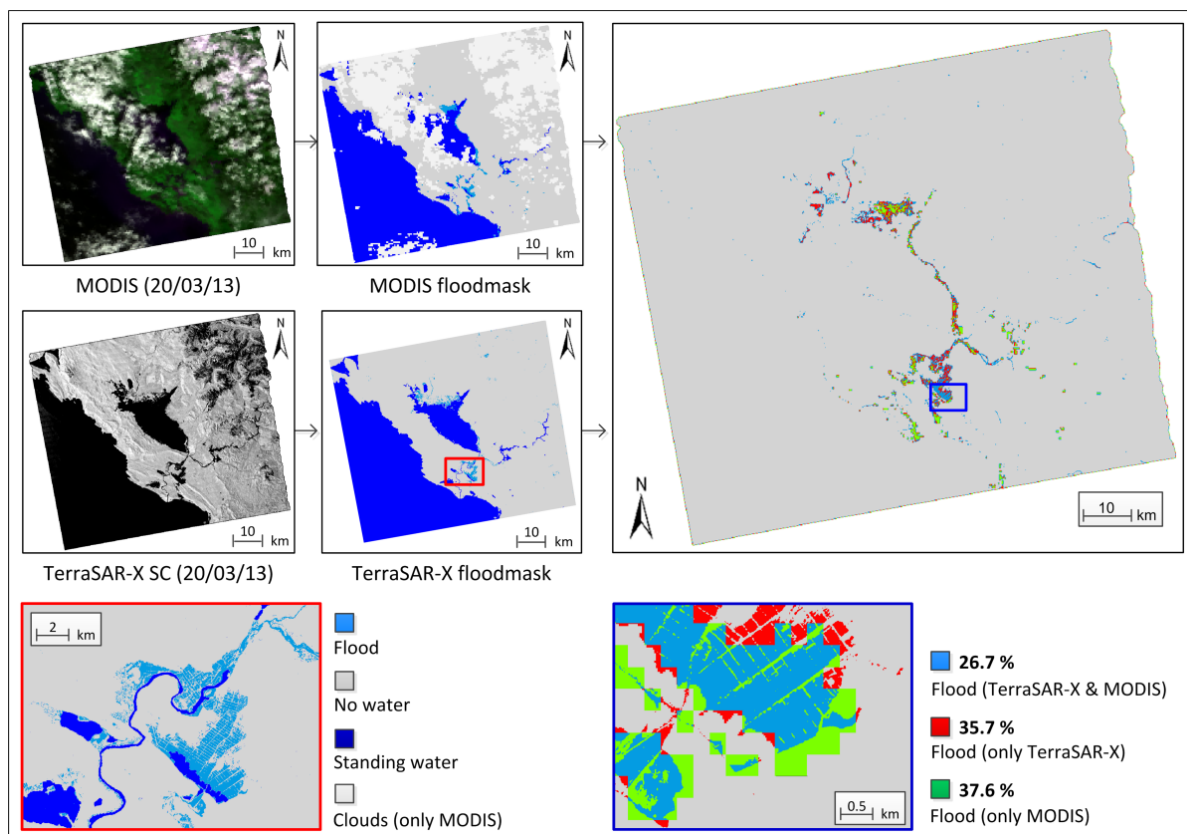
Figure 8. Correlation between flooded areas in (**a**) Russia and (**b**) Albania/Montenegro derived from MODIS and TerraSAR-X on a 2 km grid level. The regression (solid line) and trend (dotted line) of the plots are also shown.
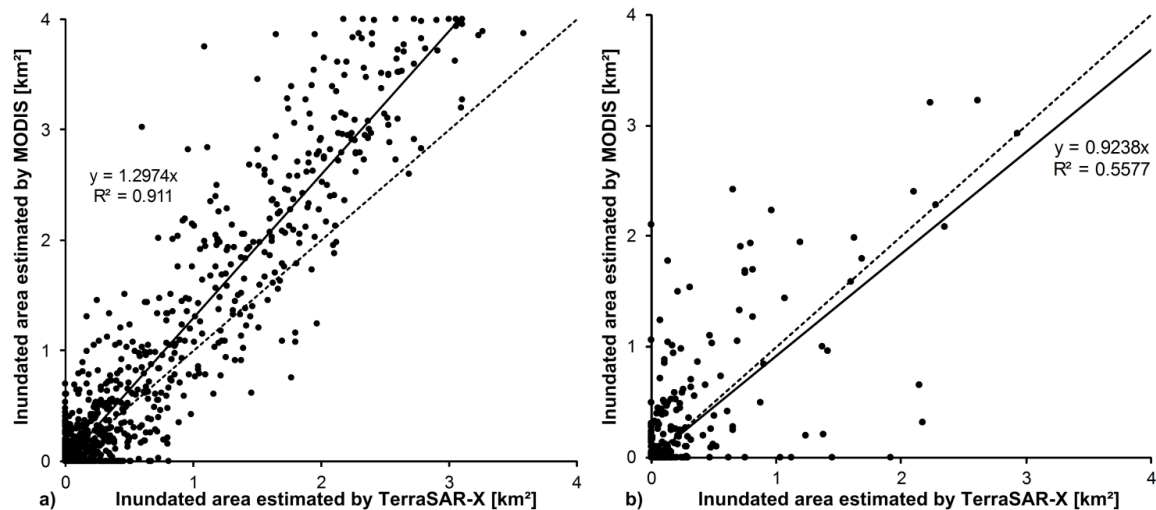
4. Conclusion

The usefulness of earth observation in crisis situations such as large-scale floods greatly depends on the timeliness of the first post-disaster satellite acquisition and the quality of subsequent data processing and product generation.

In this work we presented two fully automatic processing chains aimed to improve the timeliness of data handling and product dissemination through a combined use of both optical and radar data in flood monitoring. The classification output from systematically and daily-acquired MODIS data (monitoring mode) is used for an on demand triggering of a TerraSAR-X based flood mapping service (emergency response mode) to derive high-resolution information on the inundation extent. The methodology includes a computation and adaption of global auxiliary data (digital elevation models, topographic slope information, and reference water masks), an unsupervised initialization of the classification, a post-classification refinement, and dissemination of the crisis information via a web-based user interface.

The presented multi-scale flood monitoring system is tested for two flood scenarios in Russia and Albania/Montenegro and a cross-comparison of classification results is performed. In both scenarios, the MODIS flood mapping service was successful in identifying an evolving flood situation on a large-scale with a medium resolution of 250 m. The MODIS classification output was successfully used for on demand triggering the fully automated TerraSAR-X Flood Service (TFS), which derived high-resolution information on inundation extent of the target areas. For both scenarios, high-resolution SAR data would not have been acquired without the identification of the flooding using the MODIS Flood Service (MFS). While both classification results (optical and SAR-based) visually show a high degree of agreement, a quantitative and pixel-based evaluation indicates that the matching of classification results can vary considerably depending on several factors. These are related to data characteristics on the one hand (*i.e.*, spatial resolution, repetition rate of the satellite) and

properties of the corresponding flood situation on the other hand (*i.e.*, flood extent, complexity of the environment, cloud coverage, *etc.*).

In the presented two-scaled approach, the individual advantages of each sensor class are exploited by combining systematic and daily medium-resolution optical acquisitions for monitoring and alerting purposes with high-resolution SAR acquisitions triggered in emergency situations. To the knowledge of the authors, this is the first system which uses the near real-time classification result of a systematically acquiring satellite mission of high temporal frequency to optimize the time-critical on demand programming of high resolution SAR satellite acquisitions for detailed flood monitoring.

The MODIS-based service, although designed and tested for a global coverage, is currently only routinely operated for the European acquisition cone due to in-house and NRT data reception capabilities at the German Aerospace Center. An extension to other continents, potentially Africa and Asia, could substantially increase the relevance of the service although the integration of external data sources would be required. For further improvements in thematic accuracy of the flood services, the integration of additional ancillary variables and data sources into the classification process is considered. Using a fuzzy-based classification approach, hydrologically relevant layers, such as the topographic wetness (TWI) [40] or height above nearest drainage indices (HAND) [13,41], can be used in combination with land cover information to either assign flood probabilities to each pixel, or in combination with fixed threshold values, to filter out areas where the probability of a flood occurrence is very low. Future work also will focus on the incorporation of upcoming up-to-date global data sets of enhanced spatial resolution and accuracy in the processing chains to improve pre-processing quality and classification accuracy. The integration of, e.g., the global TanDEM-X DEM and TanDEM-X water mask (WAM) [42] with a spatial resolution of 12 m will be a significant improvement in comparison to the ASTER GDEM V2 and the SWBD.

In preparation of the Sentinel 1–3 missions, the optical and SAR-based processing chains are currently being revised and adapted. A major advantage compared to the current TerraSAR-X based approach is the systematic acquisition strategy of the Sentinel-1 mission, which allows a utilization of SAR acquisitions for continuous monitoring purposes without the necessity of time-consuming and on demand acquisition planning.

Acknowledgments

Conflicts of Interest

The authors declare no conflict of interest.

References

1. Giustarini, L.; Hostache, R.; Matgen, P.; Schumann, G.; Bates, P.D.; Mason, D.C. A change detection approach to flood mapping in urban areas using TerraSAR-X. *IEEE Trans. Geosci. Remote Sens.* **2013**, *51*, 2417–2430.

2. Martinis, S.; Twele, A.; Voigt, S. Towards operational near-real time flood detection using a split-based automatic thresholding procedure on high resolution TerraSAR-X data. *Nat. Hazards Earth Syst. Sci.* **2009**, *9*, 303–314.

3. Martinis, S.; Twele, A. A hierarchical spatio-temporal Markov model for improved flood mapping using multi-temporal X-band SAR data. *Remote Sens.* **2010**, *2*, 2240–2258.

4. Mason, D.C.; Davenport, I.J.; Neal, J.C.; Schumann, G.J.-P.; Bates, P.D. Near real-time flood detection in urban and rural areas using high-resolution Synthetic Aperture Radar images. *IEEE Trans. Geosci. Remote Sens.* **2012**, *50*, 3041–3052.

5. Matgen, P.; Hostache, R.; Schumann, G.; Pfister, L.; Hoffman, L.; Svanije, H.H.G. Towards an automated SAR based flood monitoring system: Lessons learned from two case studies. *Phys. Chem. Earth* **2011**, *36*, 241–252.

6. Schumann, G.; di Baldassarre, G.; Alsdorf, D.; Bates, P.D. Near real-time flood wave approximation on large rivers from space: Application to the River Po, Italy. *Water Resour. Res.* **2010**, *46*, 1–8.

7. Pulvirenti, L.; Chini, M.; Marzano, F.S.; Pierdicca, N.; Mori, S.; Guerriero, L.; Boni, G.; Candela, L. Detection of Floods and Heavy Rain Using Cosmo-SkyMed Data: The Event in Northwestern Italy of November 2011. In Proceedings of 2012 IEEE International Geoscience and Remote Sensing Symposium (IGARSS 2012), Munich, Germany, 22–27 July 2012; pp. 3026–3029.

8. Pulvirenti, L.; Pierdicca, N.; Chini, M.; Guerriero, L. An algorithm for operational flood mapping from Synthetic Aperture Radar (SAR) data using fuzzy logic. *Nat. Hazards Earth Syst. Sci.* **2011**, *11*, 529–540.

9. International Charter of Space and Major Disasters. Available online: http://www.disasterscharter.org/ (accessed on 6 August 2013).

10. Dartmouth Flood Observatory. Available online: http://floodobservatory.colorado.edu/ (accessed on 8 August 2013).

11. NRT Global MODIS Flood Mapping. Available online: http://oas.gsfc.nasa.gov/floodmap/ (accessed on 10 July 2013).

12. ESA Grid Processing on Demand (G-POD). Available online: http://gpod.eo.esa.int/ (accessed on 9 August 2013).

13. Westerhoff, R.S.; Kleuskens, M.P.H.; Winsemius, H.C.; Huizinga, H.J.; Brakenridge, G.R.; Bishop, C. Automated global water mapping based on wide-swath orbital synthetic-aperture radar. *Hydrol. Earth Syst. Sci.* **2013**, *17*, 651–663.

14. Auynirundronkool, K.; Chen, N.; Peng, C.; Yang, C.; Gong, J.; Silapathong, C. Flood detection and mapping of the Thailand central plain using RADARSAT and MODIS under a sensor web environment. *Int. J. Appl. Earth Obs. Geoinf.* **2012**, *14*, 245–255.

15. Mandl, D.; Cappelaere, P.G.; Frye, S.W.; Handy, M.E.; Policelli, F.; Katjizeu, M.; van Langenhove; G.; Aube, G.; Saulnier, J.-F.; Sohlberg, R.; *et al.* Use of the earth observing one (EO-1) satellite for the namibia SensorWeb flood early warning pilot. *Int. J. Appl. Earth Obs. Geoinf.* **2013**, *19*, 298–308.

16. Martinis, S.; Kersten, J.; Twele, A. A fully automated TerraSAR-X based flood service. *ISPRS J. Photogramm. Remote Sens.* **2013**, submitted.

17. Eberle, J.; Strobl, C. Web-based geoprocessing and workflow creation for generating and providing remote sensing products. *Geomatica* **2012**, *66*, 13–26.

18. Parkinson, C.L.; Greenstone, R. *EOS Data Products Handbook, Volume 2*; NASA Goddard Space Flight Center: Greenbelt, MD, USA, 2000.

19. MacDonald, M.D.; Ruebens, M.; Wang, L.; Franz, B.A. The SeaDAS Processing and Analysis System: SeaWiFS, MODIS, and Beyond. In Proceedings of the American Geophysical Union, Fall Meeting, San Francisco, CA, USA, 5–9 December 2005.

20. Goddard Space Flight Center. *MODIS Level 2 Corrected Reflectance Science Processing Algorithm (CREFL_SPA) User's Guide*; Version 1.7.1; 2010. Available online: http://directreadout.sci.gsfc.nasa.gov/links/rsd_eosdb/PDF/CREFL_1.7.1_SPA_1.1.pdf (accessed on 1 August 2013).

21. Land Processes DAAC. *MODIS Reprojection Tool Swath User Manual*; Release 2.2; Land Process Distributed Active Archive Center, USGS Earth Resources Observation and Science (EROS) Center: Sioux Falls, SD, USA, 2010. Available online: https://lpdaac.usgs.gov/sites/default/files/public/MRTSwath_Users_ Manual_2.2_Dec2010.pdf (accessed on 1 August 2013).

22. Carroll, M.; Townshend, J.; DiMiceli, C.; Noojipady, P.; Sohlberg, R. A new global raster water mask at 250 meter resolution. *Int. J. Digit. Earth* **2009**, *2*, 291–308.

23. De Groeve, T.; Vernaccini, L.; Brakenridge, G.R.; Adler, R.; Ricko, M.; Wu, H.; Thielen, J.; Salamon, P.; Policelli, F.S.; Slayback, D.; *et al. JRC Technical Reports: Global Integrated Flood Map*; JRC80255; Publications Office of the European Union: Luxembourg, 2013.

24. Aster GDEM V2. Available online: https://lpdaac.usgs.gov/get_data (accessed on 8 April 2013).

25. Jähne, B.; Scharr, H.; Körkel, S. Principles of Filter Design. In *Handbook of Computer Vision and Applications*; Academic Press: London, UK, 1999.

26. Sakamoto, T.; Nguyen, N.V.; Kotera, A.; Ohno, H.; Ishitsuka, N.; Yokozawa, M. Detecting temporal changes in the extent of annual flooding within the Cambodia and the Vietnamese Mekong Delta from MODIS time-series imagery. *Remote Sens. Environ.* **2007**, *109*, 366–374.

27. Islam, A.S.; Bala, S.K.; Haque, M.A. Flood inundation map of Bangladesh using MODIS time-series images. *J. Flood Risk Manag.* **2010**, *3*, 210–222.

28. Yan, Y.-E.; Ouyang, Z.-T.; Guo, H.-Q.; Jin, S.-S.; Zhao, B. Detecting the spatiotemporal changes of tidal flood in the estuarine wetland by using MODIS time series data. *J. Hydrol.* **2010**, *384*, 156–163.

29. Huete, A.R.; Liu, H.Q.; Batchily, K.; van Leeuwen, W. A comparison of vegetation indices global set of TM images for EOS-MODIS. *Remote Sens. Environ.* **1997**, *59*, 440–451.

30. Huete, A.R.; Didan, K.; Miura, T.; Rodriguez, E.P.; Gao, X.; Ferreira, L.G. Overview of the radiometric and biophysical performance of the MODIS vegetation indices. *Remote Sens. Environ.* **2002**, *83*, 195–213.

31. Zhang, R.; Sun, D.; Li, S.; Yu, Y. A stepwise cloud shadow detection approach combining geometry determination and SVM classification for MODIS data. *Int. J. Remote Sens.* **2013**, *34*, 211–226.

32. Li, S.; Sun, D.; Yu, Y. Automatic cloud-shadow removal from flood/standing water maps using MSG/SEVIRI imagery. *Int. J. Remote Sens.* **2013**, *34*, 5487–5502.

33. Luo, Y.; Trishchenko, A.P.; Khlopenkov, K.V. Developing clear-sky, cloud and cloud shadow mask for producing clear-sky composites at 250-meter spatial resolution for the seven MODIS land bands over Canada and North America. *Remote Sens. Environ.* **2008**, *112*, 4167–4185.

34. Simpson, J.J.; Jin, Z.H.; Stitt, J.R. Cloud shadow detection under arbitrary viewing and illumination conditions. *IEEE Trans. Geosci. Remote Sens.* **2000**, *38*, 972–976.

35. Hutchinson, K.D.; Mahoney, R.L.; Vermote, E.F.; Kopp, T.J.; Jackson, J.M.; Sei, A.; Iisager, B.D. A geometry-based approach to identifying cloud shadows in the VIIRS cloud mask algorithm for NPOESS. *J. Atmos. Ocean. Technol.* **2009**, *26*, 1388–1397.

36. Kuenzer, C.; Guo, H.; Schlegel, I.; Tuan, V.Q.; Li, X.; Dech, S. Varying scale and capability of envisat ASAR-WSM, TerraSAR-X Scansar and TerraSAR-X Stripmap data to assess urban flood situations: A case study of the Mekong delta in Can Tho province. *Remote Sens.* **2013**, *5*, 5122–5142.

37. Infoterra. *Radiometric Calibration of TerraSAR-X Data*; Infoterra GmbH: Friedrichshafen, Germany, 2008. Available online: http://www.astrium-geo.com/files/pmedia/public/ r465_9_tsxx-itd-tn-0049-radiometric_calculations_i1.00.pdf (accessed on 29 July 2013).

38. SWBD. *Shuttle Radar Topography Mission Water Body Data Set*; 2005. Available online: http://dds.cr.usgs.gov/srtm/version2_1/SWBD/ (accessed on 28 August 2013).

39. Kittler, J.; Illingworth, J. Minimum error thresholding. *Pattern Recognit.* **1986**, *19*, 41–47.

40. Beven, K.J.; Kirkby, M.J. A physically based, variable contributing area model of basin hydrology. *Hydrol. Sci. Bull.* **1979**, *24*, 43–69.

41. Rennó, C.D.; Nobre, A.D.; Cuartas, L.A.; Soares, J.V.; Hodnett, M.G.; Tomasella, J.; Waterloo, M.J. HAND, a new terrain descriptor using SRTM-DEM: Mapping terra-firme rainforest environments in Amazonia. *Remote Sens. Environ.* **2008**, *112*, 3469–3481.

42. Wendleder, A.; Wessel, B.; Roth, A.; Breunig, M.; Martin, K.; Wagenbrenner, S. TanDEM-X water indication mask: Generation and first evaluation results. *IEEE J. Sel. Top. Appl. Earth Obs. Remote Sens.* **2013**, *6*, 171–179.